Environmental Science Nano

ROYAL SOCIETY OF CHEMISTRY

PAPER

View Article Online
View Journal | View Issue

Cite this: *Environ. Sci.: Nano*, 2026, **13**, 280

Magnetically controllable sponges for crude oil, mercury, and arsenic removal

Panagiota Bika,[a] Nadia Todorova,[a] Maria-Anna Gatou,[b] Michael Pissas,[a] Eamonn Devlin,[a] Elias Sakellis,[ac] Nikos Boukos,[a] Nefeli Lagopati,[d] Theopisti Lymperopoulou,[e] Lamprini-Areti Tsakanika,[e] Evangelia A. Pavlatou,[b] Vasileios K. Tzitzios [a] and Panagiotis Dallas *[af]

In this work, we present three different pathways to render commercial melamine sponges, both magnetic and hydrophobic, thereby offering them the capacity to effectively and selectively remove crude oil and heavy metals from aqueous environments. The magnetic properties were endowed by the deposition of as-synthesized iron oxide nanoparticles, functionalized with hydrophobic oleic acid and oleylamine ligands, *via* a large-scale synthesis. Aiming for an even higher hydrophobicity, terminal vinyl groups were attached to the pristine and modified sponges through a sol–gel hydrolysis of VTES@SiO_2. The magnetic materials were thoroughly characterized and evaluated for their efficiency in water purification applications, regarding the adsorption of crude oil and heavy metal pollutants. Each pathway of preparation was effectively practical for a different application. The initial coating of the sponges with a hydrophobic layer (Sp-h-m) enhanced the adsorption and the retention of iron oxide nanoparticles, resulting in materials with a maximum magnetization of 25 × 10^{-3} emu. This modified sponge also exhibited the highest removal of metal ions (As^{3+} and Hg^{2+}) from aqueous solutions within 60 minutes, and its extraction efficiency was evaluated in systems with single metal ions (250 ppm) and in the removal of metal ions (As^{3+} and Hg^{2+}) from aqueous solutions within the same time frame. It was evaluated for its extraction efficiency in systems with single metal ions (250 ppm) and under competitive conditions (500 ppm of toxic metals in total). The coating with a hydrophobic layer, following the deposition of the magnetic nanoparticles (Sp-m-h), led to further improvement of the sponge's hydrophobicity (from 129° to 140° water contact angle; WCA), excellent selectivity to crude oil, and water repellency. The magnetically modified sponges exhibited significant initial adsorption capacities (60–100 g g^{-1}) and average adsorption capacities (35–65 g g^{-1}) over 15 cycles. The high selectivity, adsorption/desorption efficiency (up to 99.8%), their adsorption capacity for As and Hg metal ions and their responses to external magnetic fields confirmed the suitability of the developed magnetic sponges for water purification systems. The versatility of the proposed modification route allows the preparation and optimization of specific magnetic sponges for targeted applications.

Received 12th June 2025,
Accepted 7th November 2025

DOI: 10.1039/d5en00549c

rsc.li/es-nano

Environmental significance

Melamine sponge is an excellent absorbing material, non-toxic and low cost, with chemical and mechanical stability. Its 3D porous structure possesses functional groups, allowing its effective modification with other nanomaterials to obtain targeted properties, such as magnetic response and hydrophobicity. We propose versatile routes for the modification of the sponge, aiming to develop composite materials that deal with the pollutants of oil and heavy metal ions in aqueous environments. The modifiers, based on magnetic iron oxide and silica nanoparticles, are not only environmentally friendly by composition, without toxic halogen components, but they are also attached to the sponges' matrix, thus avoiding any secondary pollution. Through remote navigation, the magnetic hydrophobic modified sponges offer safe decontamination of water under extreme or hazardous conditions.

[a] *Institute of Nanoscience and Nanotechnology, NCSR Demokritos, 15341, Athens, Greece. E-mail: pdallas@eie.gr, p.dallas@inn.demokritos.gr*
[b] *Laboratory of General Chemistry, School of Chemical Engineering, National Technical University of Athens, Zografou Campus, 15772, Athens, Greece*
[c] *Department of Physics, National and Kapodistrian University of Athens, Athens, Greece*
[d] *Laboratory of Biology, Department of Basic Medical Sciences, Medical School, Biomedical Research Foundation, Academy of Athens, National and Kapodistrian University of Athens, 11527 Athens, Greece*
[e] *Laboratory of Inorganic and Analytical Chemistry, School of Chemical Engineering, National Technical University of Athens, Polytechniopolis Zografou, Iroon Polytechniou 9, 15780 Athens, Greece*
[f] *Theoretical and Physical Chemistry Institute, National Hellenic Research Foundation, 11635 Athens, Greece*

1. Introduction

Nowadays, water contamination with crude oil and heavy metals is a critical issue threatening both aquatic ecosystems and humans.[1,2] One of the most effective and environmentally friendly techniques that is currently employed for oil removal is the physical adsorption by sponge-based materials which are lightweight, low-cost and have a stable 3D network structure with high-void fraction.[3–5] These requirements are primarily encountered in polyurethane[6–9] and melamine sponges,[10–12] and to some extent in carbon-based,[13] silicon,[14] and wood[15] adsorbers.

The melamine sponge is receiving great attention because of its availability, high elasticity and capacity. It should be noted that in the literature the performance of the sponge materials is expressed by both "absorption" and "adsorption" capacity due to the processes of holding oil within their volume (pores and channels) and the adherence of the oil to the sponge surface, especially after modification. In the present work, the term "adsorption" capacity was adopted for the general discussion and for the presentation of the results to emphasize the performed surface modification. It is known that surface functional groups such as hydroxyl (–OH), amino ($-NH_2$), and secondary amine (–NH) groups are important features, which can be engaged either in chemical reactions (*e.g.* silanization) or in the attachment of various nanoparticles to endow specific properties.[16] For oil removal applications, a high selectivity to oil and simultaneous water repellency is targeted by altering the sponges' roughness and surface energy as well as a high stability over multiple sorption/desorption cycles without any secondary pollution of the treated water. Therefore, melamine sponges possessing inherent hydrophilicity and oleophilicity are being modified with hydrophobic components and functional nanoparticles to become highly selective for oil compounds as well as to respond to external stimuli (*e.g.*, magnetic field, light) when appropriate. Beyond hydrophobicity, additional magnetic, photothermic, anti-icing, *etc.* properties have been pursued. Modifiers such as silanes,[14,17] hydrophobic polymers,[18,19] nanoparticles of titania and iron oxide,[20–23] two-dimensional MXenes and carbon nanomaterials (graphene, reduced graphene oxide)[6,24,25] as well as combinations of them[26–28] have been investigated. Adsorption capacities ranging from 4 to 240 g g^{-1} (g oil per g sponge) and hydrophobicity between 120° and 169° WCA) have been achieved, depending on the selected agents and modification methods. Synthetic procedures, such as dip-coating,[17,18,29,30] *in situ* growth of nanoparticles,[31] and polymerization[32,33] as well as solvothermal treatment[34] and sol–gel,[35] have been employed. Among those, sol–gel and dip-coating impregnation with or without thermal curing appeared to be the most frequently used[16] due not only to the relatively high selectivity (140°–150°) and adsorption capacities (50–140 g g^{-1}) achieved but also to the mild conditions and cost-effective, scalable processing.

Multifunctional magnetic superhydrophobic melamine sponges are being developed for oil–water separation processes to enhance the adsorption capacity and selectivity towards oil as well as the capacity to operate in hazardous conditions and respond remotely. Iron oxide nanoparticles are prominent candidates for these applications when combined with hydrophobic compounds and incorporated into the desired matrix. The stability of these composites is an additional parameter that needs to be addressed not only to ensure the reusability of the sponge but also to avoid side pollution of the water with hazardous compounds and nanoparticles. In the literature, numerous reports exist on magnetic (super) hydrophobic oil-adsorbing melamine sponges. For example, magnetic nanoparticles have been synthesized in one-pot solvothermal reaction of iron precursor and various hydrophobic substances, although some of them are F-containing silane (*e.g.*, 1*H*,1*H*,2*H*,2*H*-heptadecafluorodecyltriethoxysilane).[34] In that work, bonding between the magnetic nanoparticles and the melamine sponge was achieved using a silicon adhesive, reaching maximum adsorption capacities ranged from 39.8 g g^{-1} (pump oil) to 78.7 g g^{-1} (silicone oil). Following a similar approach, a magnetically responsive and superhydrophobic sponge was developed,[29] where a ferroferric oxide nanoparticle/graphene oxide hybrid was solvothermally prepared and then hydrophobically modified with a perfluorinated silane. The composite was anchored onto a melamine sponge, resulting in a superhydrophobic (163° WCA)/superoleophilic (0° OCA) material that exhibits selective adsorption of various oils between 63 and 156 g g^{-1} with good recyclability. In a more environmentally friendly approach, magnetic Fe_3O_4 nanoparticles were coupled with selected non-toxic deep eutectic solvents (DES@Fe_3O_4)[30] for a 101.7–127.3 g g^{-1} adsorption capacity of real crude oils. A different route has been suggested[26] with a two-step modification route, where Fe_3O_4 and WS_2 nanoparticles were first deposited on the melamine sponge, and then a polydopamine/*n*-octadecanethiol film was built to obtain a rough hydrophobic (156.8 WCA) structure with low surface energy. As a result, an adsorption capacity of 40–100 g g^{-1} and good reusability were obtained. Polydopamine has also been used[27] in combination with 3-aminopropyltriethoxysilane to achieve a 158.3° WCA and an adsorption capacity of 43.2–80.7 g g^{-1}. Thus, it is evident that the efficiency and the environmental appropriateness of the magnetic hydrophobic sponges are strongly dependent on (i) the interplay between the two parts, *i.e.* selected hydrophobic substance and magnetic nanoparticles, (ii) the *in situ* or subsequent modification of the nanoparticles, and (iii) the selected sequence of nanoparticle deposition and stabilization processes.

Apart from the extraction of oil, sponges are often suggested for the removal of heavy metal ions (Hg^{2+}, Pb^{2+}, As^{3+}, Cd^{2+}, *etc.*).[36,37] A super-amphiphilic silicon sponge was reported to adsorb a high amount of Hg^{2+} from a water solution with concentrations between 63 and 6231 ppm. Nevertheless, an efficiency of 98% to 99% is achieved depending on the concentration. These results are related to the porosity of the sponge and the strong affinity between Hg^{2+} and the sulfur atoms in the network skeleton.[14] A polyurethane sponge modified with reduced graphene oxide was also examined for both oil–water separation and the

removal of hazardous metal ions (Cu^{2+}) from wastewater.[6] The PU@rGO sponge exhibited a ~100% removal within 2 h at low Cu^{2+} concentrations (6 ppm). Most importantly, magnetic nanoparticles, when dispersed in water, can effectively remove Pb^{2+} and Cr^{6+} through electrostatic mechanisms, as reported by Wang *et al.*[38]

In the present work, a low-cost, commercially available melamine sponge was used for the preparation of ecologically friendly magnetic hydrophobic adsorbers for the removal of crude oil and heavy metal ions from water. A thermolytic one-step reaction was employed for the synthesis of hydrophobic iron oxide nanoparticles in organic solvents before the main dip-coating modification procedure of the sponges in the stable colloidal suspension Aiming for a greater water repellency and a high adsorption efficiency, an additional sol–gel silanization with hydrophobic vinyl ligands was applied before and after the deposition of the magnetic nanoparticles, thus altering the functional terminations on the sponge's surface. The prepared magnetic–hydrophobic melamine sponges were characterized and evaluated for both crude oil and heavy metal ion (Hg^{2+}, As^{3+}) removal from water. The influence of the attached magnetic (Fe_3O_4) and hydrophobic (VTES@SiO_2) nanoparticles and their synergetic effects as well as the sequence of the modification processes of the modified sponges were evaluated on the crude oil and metal selectivity.

2. Experimental section

2.1. Materials

The commercial Wevora WR-009 melamine sponge was employed as a substrate. Tetraethylorthosilicate (98%, $Si(OC_2H_5)_4$, TEOS) was purchased from Arcos and absolute ethanol (99.8%) from Thermo Fisher. Ammonia solution (25%, NH_4OH) and *n*-hexane (99%) were purchased from Carlo Erba, while triethoxyvinylsilane (97%, $C_8H_{18}O_3Si$, VTES) and oleic acid (90%, $C_{18}H_{34}O_2$, OA) were from Thermo Scientific. Iron(III) acetylacetonate (70%, $Fe(C_5H_7O_2)_3$), oleylamine (70%, $C_{18}H_{35}NH_2$, OLE), arsenic(III) chloride (99.99%, $AsCl_3$), mercury(II) chloride (≥99.5%, $HgCl_2$), mercury standard for AAS (1 g L^{-1} Hg in nitric acid), and arsenic standard for AAS (1 g L^{-1} As in nitric acid) were acquired from Sigma Aldrich.

2.2. Synthesis of iron oxide nanoparticles (sample: NPs)

The nanoparticles were synthesized following a slightly modified, previously reported work.[39] In a typical experiment, 4 g Fe^{3+} in acetylacetonate salt form was dissolved in a mixture of 19 mL oleylamine and 1 mL oleic acid. Thermolytic synthesis was performed. The mixture was stirred under reflux and the temperature was raised to 250 °C. The reaction proceeded for 2 h and the solution was cooled to room temperature. Afterwards, 50 mL of ethanol was added to the iron oxide nanoparticles solution to precipitate the formed nanoparticles, which were effectively collected through a magnetic separation procedure. The suspension was disposed of and the process was repeated three times to purify the iron oxide nanoparticles from any remaining oleylamine on the nanoparticles' surface. The large-scale synthesis was accomplished, and 1 g organophilic iron oxide nanoparticles were dispersed and stored in hexane. The final concentration of the hexane solution was set at 10 mg mL^{-1}.

2.3. Preparation of magnetic sponges (sample: Sp-m)

The melamine sponge was cut into pieces with dimensions of 2 cm × 2 cm × 0.5 cm, and 10 mg mL^{-1} iron oxide NP hexane solution was used for its immersion. They were submitted to a multiple compression/decompression procedure that was manually applied to ensure the infusion of the nanoparticles into the pores of the sponge. Then, the sponges were dried at 60 °C in an oven for 24 h to evaporate any remaining solvent and further stabilize the iron oxide nanoparticles on the sponge. This type of magnetic sponge is denoted as Sp-m.

2.4. Preparation of magnetic and hydrophobic sponges (sample: Sp-h-m)

The melamine sponges were cut into pieces with dimensions of 2 cm × 2 cm × 0.5 cm for this preparation procedure as well. A sol–gel process was selected for the synthesis of silica nanoparticles adsorbed on the skeleton of the melamine sponges. A similar procedure to that of Gao *et al.*[11] was followed: 4 mL of TEOS was added to 40 mL of absolute ethanol under stirring under ambient conditions. Then, 1.6 mL NH_4OH was added, and the solution was kept under stirring for 48 h under ambient conditions for the successive hydrolysis and the formation of SiO_2 nanoparticles. Subsequently, the pristine sponges were impregnated with the mixture for 6 h. After the first modification step, the SiO_2 sponges were rinsed with ethanol to remove excess silica nanoparticles, and they were then introduced into a solution containing the silane coupling hydrophobic agent. The latter consisted of 40 mL of absolute ethanol with 4 mL of VTES and 1.6 mL of ammonia solution. The sponges remained under stirring for 24 h. After their removal, the sponges were rinsed with ethanol and air-dried at room temperature. They were then further submitted to the same process as the Sp-m sample, including immersion and compression/decompression cycles in the iron oxide nanoparticles' solution—the procedure ended by drying the samples at 60 °C in an oven for 24 h. The new composite sponge is denoted as Sp-h-m.

2.5. Preparation of superhydrophobic and magnetic sponges (sample: Sp-m-h)

The magnetic sponges, sample Sp-m, were also subjected to the silanization process with VTES for the synthesis of superhydrophobic magnetic sponges. Namely, the Sp-m sponges were immersed for 6 h in the TEOS/NH_4OH/ethanol solution, which had been previously hydrolyzed for 48 h. They were rinsed with ethanol before their transfer in the VTES/NH_4OH/ethanol solution, where they remained under

stirring for 24 h. The final sponges, denoted as Sp-m-h, were rinsed with ethanol and dried at room temperature.

2.6. Evaluation of crude oil removal from water

The performance of pristine and modified sponges in removing crude oil from aqueous environments was evaluated using sponge pieces with dimensions of 1 cm × 1 cm × 0.5 cm. Their oil selectivity, adsorption capacity, and reusability were assessed in water/oil systems with different amounts of oil. Specifically, for the selectivity evaluation, 60 g of water and 0.5 g of crude oil were placed in plastic containers where oil spots were formed on the water surface due to their immiscibility. The sponges were added to the oil/water system, which was stirred at 300 rpm for 60 min. Then, the sponges were removed from the containers, pressed to release the adsorbed quantity and returned to the oil/water systems. This procedure was repeated 6 times. For each cycle, the weight of the sponges was recorded before and after the adsorption.

For the assessment of adsorption capacity and reusability, oil-rich systems composed of 60 g of water and 10 g of crude oil were prepared. In this case, a thick oil layer completely covering the water surface was formed. The sponges were added to the systems and remained under stirring for 30 min. Similarly, the sponges were removed, pressed to release the adsorbed oil and returned to the system. The sorption–desorption procedure was performed 15 times. For each cycle, the weight of the sponges before the adsorption (pressed) and after the adsorption (with the adsorbed oil) was recorded. The values were used to calculate the adsorption capacity (AC) using eqn (1) and (2):

$$\mathrm{AC}_{m/m} = \frac{m_\mathrm{a} - m_\mathrm{b}}{m_\mathrm{b}}, \left[\mathrm{g\ g^{-1}}\right] \quad (1)$$

$$\mathrm{AC}_{m/V} = \frac{m_\mathrm{a} - m_\mathrm{b}}{V_\mathrm{s}}, \left[\mathrm{g\ cm^{-3}}\right] \quad (2)$$

where m_b is the mass of the sponge before adsorption (pressed), m_a is the mass of the sponge after adsorption (with the adsorbed oil) and V_s is the volume of the sponge (0.5 $\mathrm{cm^3}$).

2.7. Evaluation of heavy metal ion removal from water

Furthermore, both pristine and modified sponges were evaluated regarding their ability to remove heavy metal ions (*i.e.* Hg^{2+} and As^{3+}) from single metal ion aqueous solutions under dynamic conditions. The dynamic adsorption experiments were carried out using an experimental set-up of three small-scale columns, using 5 mL PVC syringes, filled with the tested sponges. The sponges were arranged in a particular way to obtain a uniform bed height. Three columns were prepared for each sample to examine the reproducibility of the experimental results. They were adjusted to three-channel micro-flow variable-speed peristaltic pumps (BQ80S, LeadFluid Co. Ltd) *via* silicon pipes, enabling the simultaneous upward inlet of the solutions into 3 columns. The columns were washed with double deionized water prior to adsorption experiments with an upward flow equal to 0.07 mL $\mathrm{min^{-1}}$ (0.5 rpm) for 24 h to remove any soluble salts and stabilize the bed porosity. Afterwards, the adsorption efficiency of the sponges regarding the Hg^{2+} and As^{3+} was evaluated using an initial metal ion concentration equal to 250 mg $\mathrm{L^{-1}}$ and an upward flow mode of the inlet solution with a rate equal to 0.35 mL $\mathrm{min^{-1}}$. To assess the selectivity between the two heavy metals, an experiment with both arsenic and mercury cations at a concentration of 250 mg $\mathrm{L^{-1}}$ each was performed. The examined flow rate was selected based on the size of the columns, the permeability of the beds and laboratory trials. The experiments were conducted at ambient temperature and the effluents were collected from the top of the columns. The collected effluents were stored at 4 °C prior to analysis *via* F-AAS, using an external calibration method on a PerkinElmer PinAAcle 500 series flame atomic absorption spectrometer. The procedure followed is given in detail in the subsection of the heavy metal ions' evaluation.

3. Characterization techniques

The chemical composition was evaluated through FTIR spectra, which were recorded on a Thermo Nicolet iS50 instrument in attenuated total reflection mode from 400 $\mathrm{cm^{-1}}$ to 4000 $\mathrm{cm^{-1}}$. The crystalline structure was analyzed using X-ray diffraction (XRD) patterns from 2° to 80° (2θ), which were obtained with a Smart Lab Rigaku diffractometer (Cu Ka radiation). The surface morphologies were analyzed with scanning electron microscopy (SEM) using a JEOL 7401f field emission SEM and the samples were sputter-coated beforehand with Au. For the size, shape and distribution of the iron oxide nanoparticles, an FEI Talos F200i field-emission (scanning) transmission electron microscope (Thermo Fisher Scientific Inc., Waltham, MA, USA) was used and the nanoparticles were drop casted from hexane solution on copper grids for the analysis. The TEM was operated at 200 kV and equipped with a windowless energy-dispersive spectroscopy microanalyzer (6T/100 Bruker, Hamburg, Germany). Mössbauer spectra were collected using a conventional transmission spectrometer with a ^{57}Co(Rh) source moving with constant acceleration at RT. Isomer shifts are given with respect to metallic iron at RT. The spectra were least-squares fitted using the IMSG program.[40] The magnetization curves were recorded on a DXV-220 vibrating sample magnetometer (VSM) with the external magnetic field varying from −10 to 10 kOe. The surface wettability was evaluated through an Ossila contact angle goniometer.

4. Results and discussion

4.1. Iron oxide nanoparticles and magnetically modified sponges

Nanophase magnetic iron oxide nanoparticles were synthesized and coated under a thermolytic reaction in the presence of OA and OLE as ligands. Afterwards, they were incorporated into either pristine or modified melamine sponges, according to the procedure described in detail in the Experimental section and presented in Scheme 1.

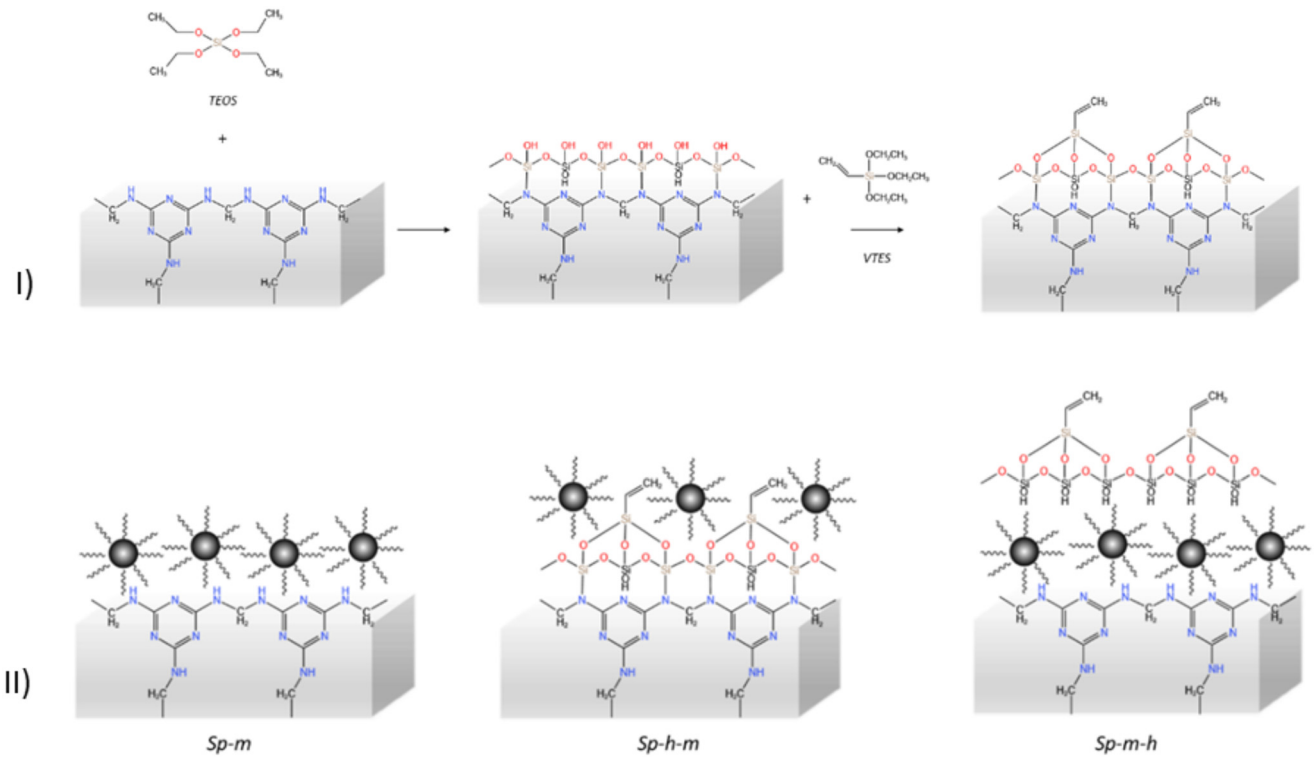

Scheme 1 Illustration of (I) the sol–gel process for the synthesis of hydrophobic coating and (II) the functionalized (the representations of the ligands with curved lines) magnetic nanoparticles (black spheres) in either the pristine sponge or the organophilic sponges.

The OA and OLE ligands employed in this work are widely used for the synthesis of colloidal nanoparticles.[41] Oleylamine is used as a high-boiling-point solvent, thermolytic, and capping agent,[39] while the addition of oleic acid provides higher stability to the final nanoparticles, specifically for non-polar solvents. The organic layer encapsulating the nanoparticles prevents their aggregation and offers them solubility in organic solvents through the growth of hydrophobic interactions between the aliphatic chains of OA and OLE. The magnetic behavior of the organophilic nanoparticles' dispersion was examined using a permanent magnet, as shown in Fig. S1, where their ferrofluid behavior is presented, confirming the successful synthesis.

The crystalline nature of the as-synthesized nanoparticles was evaluated by XRD analysis. This technique cannot distinguish between the oxide types of nanoparticles, specifically the formation of either magnetite (Fe_3O_4) or maghemite (γ-Fe_2O_3), as both have a cubic spinel structure. In Fig. 1a, we present the XRD patterns of the nanoparticles in comparison with the diffraction peaks of magnetite (JCPS: 96-900-5839) and maghemite (JCPS: 96-900-6317). The diffractogram reveals the reflections at 30.23° (202), 35.57° (311), 43.25° (400), 54.02° (422), 57.2° (511), and 62.93° (440). From the most intense reflection, the average crystallite size of the surface-modified nanoparticles was calculated using an XRD analysis software according to the Scherrer equation: $D = K\lambda/(\beta \cos\theta)$, where D is the crystallite size, K is the Scherrer constant, β is the full-width at half-maximum (FWHM), and θ is the Bragg diffraction angle.[42] The calculated average crystallite size, as determined by the equation, is ~8 nm for the iron oxide nanoparticles. In Fig. 1b, TEM images at a 100 nm and 50 nm scale present the various geometries of the synthesized nanoparticles. Their size fluctuates from 6 nm to 17 nm and a representative size distribution diagram can be seen in Fig. S2. The synthesis and the *in situ* functionalization of the iron oxide nanoparticles did not cause any aggregation in the suspension. Their shape is polyhedral, and it is a natural evolution of their nucleation and growth under the synthetic conditions used.[43]

It is well known that the ratio of Fe^{2+} and Fe^{3+} cations during the synthesis can influence the ratio of magnetite and maghemite phases in iron oxide nanoparticles.[44,45] Mössbauer spectroscopy is a powerful tool for identifying the phase composition in as-synthesized nanoparticles. As magnetite is easily oxidized to maghemite with time, directly after their synthesis the nanoparticle solution was frozen to 125 K for the measurement. Thus, we expect minimal oxidation. The experimental spectrum along with theoretical simulations are plotted and presented in Fig. 1c. The sample can be fitted using three well-defined and one broadened sextet (Table 1). The spectrum, obtained at 125 K, has a characteristic asymmetry associated with magnetite, allowing the sextets to be assigned to magnetite A (one sextet) and B (three sextets) sites by their distinctive isomer shift values. The subspectral areas of the sextets yield an A : B area ratio of 1 : 1.85. This differs but only slightly from that expected from well-crystallised stoichiometric magnetite, 1 : 2. This observation combined with the broad range of the three subspectra associated with the B site

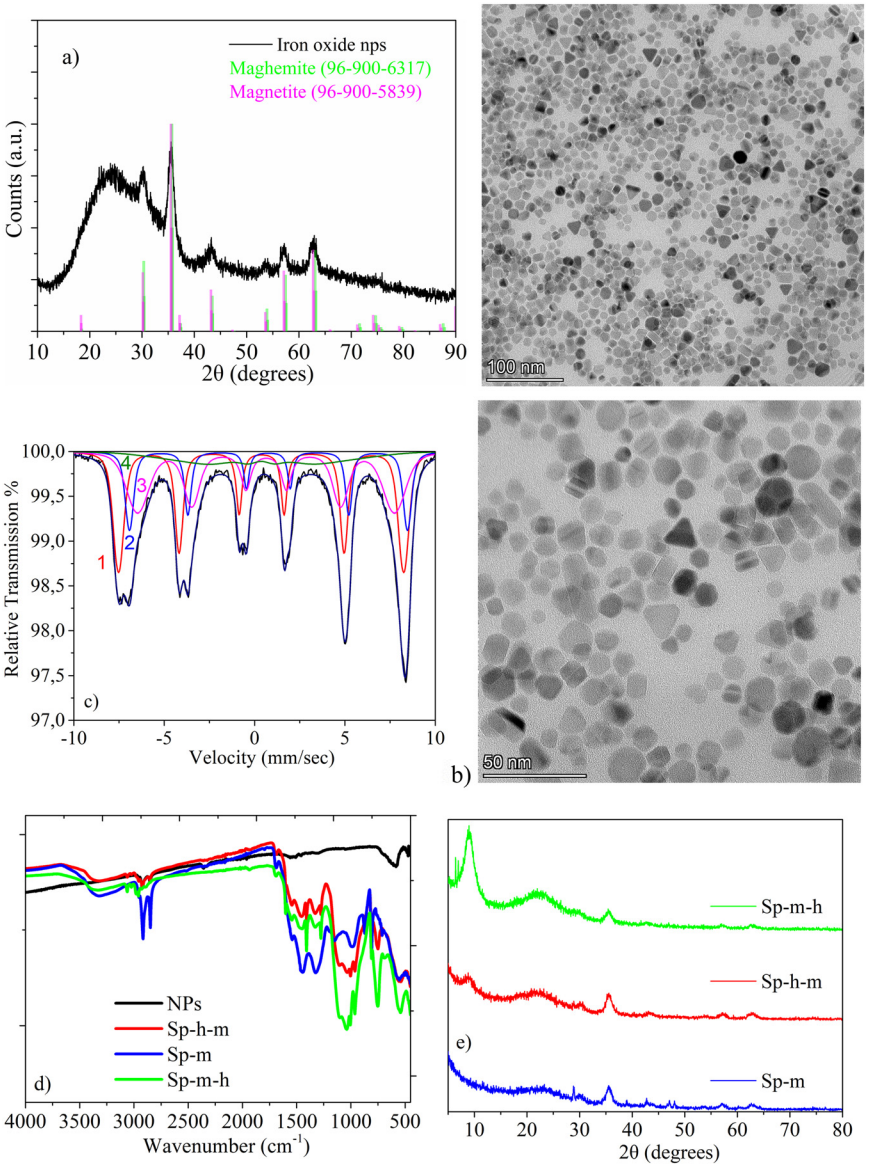

Fig. 1 (a) The XRD pattern, (b) TEM images, and (c) the Mössbauer spectrum of the iron oxide NPs (non-stoichiometric magnetite), (d) the FT-IR spectra of all the evaluated materials (non-stoichiometric magnetite NPs and the modified sponges), and (e) the XRD patterns of the three modified sponges.

indicates that the sample is composed of non-stoichiometric magnetite.

Regarding the chemical composition of the capped magnetic nanoparticles, FTIR analysis is provided in Fig. 1d. The intense vibrations at the high frequencies of 2956 cm^{-1} are assigned to the C–H mode, and those at 2920 cm^{-1} and 2852 cm^{-1} are ascribed to the symmetric and asymmetric $–CH_2–$ vibrations of the aliphatic chains of oleic acid and oleylamine.[46] These peaks, in comparison with the pure oleic acid, are slightly shifted towards lower frequencies due to adsorption to the solid surface and the close packing of hydrocarbon molecules surrounding the nanoparticles.[47] Meanwhile, the stretching vibration of the –N–H in oleylamine on the nanoparticles' surface is not evident at the expected wavenumber of 3322 cm^{-1} due to its low intensity. The adsorptions centered at 1558 cm^{-1} and 1457 cm^{-1} are attributed to the asymmetric and symmetric stretching vibrations of the bidentate –COO group, respectively.[46] The presence of both carboxylate bands confirms the attachment of oleic acid on the surface of the nanoparticles. A low-

Table 1 Mössbauer simulation parameters for the spectrum of iron oxide nanoparticles recorded at 125 K

Subspectrum	Site	Isomer shift (MM s^{-1})	Hyperfine field (kG)	Area (%)
1	A	0.38(5)	490(3)	35(3)
2	B	0.77(5)	478(3)	20(3)
3	B	0.64(5)	441(5)	35(3)
4	B	0.7(1)	279(10)	10(5)

intensity peak at 1296 cm^{-1} corresponds to the –C–O stretch, while the intense band of the characteristic –C═O asymmetric band of oleic acid is absent, verifying the bridged conjugation. At lower frequencies, the strong adsorption at 584 cm^{-1} is attributed to the Fe–O bond, which indicates the formation of an iron oxide network with oleate groups bridged on its surface.[48]

Afterwards, the NPs were incorporated into either a pristine sponge or one coated with a hydrophobic silane agent.[49] FT-IR analysis was conducted to confirm the chemical modifications (Fig. 1e). The FTIR results reveal the characteristic adsorption bands of the pristine sponge at 809 cm^{-1} (bending vibration) and at 1546 cm^{-1} (C═N stretching vibration). The peaks at 1331 cm^{-1} and 1448 cm^{-1} correspond to the –C–H bending vibrations. The peaks at 1689 cm^{-1} are assigned to C═C mode, and at 2848 cm^{-1}, 2916 cm^{-1}, and 2958 cm^{-1} are attributed to the –CH2 symmetric asymmetric and C–H vibrations.[49] In all magnetically modified sponges, the Fe–O vibrational mode appears at 562 cm^{-1}. In contrast, in the hydrophobically modified sponges, vibrations assigned to the vinyl characteristic groups[11] occur at 2980 cm^{-1} (–C–H), 3022 cm^{-1} (C–H), and 3061 cm^{-1} (═C–H). Additionally, others evolved at 1601 cm^{-1}, indicative of the –CH═CH2 stretching, 1409 cm^{-1} for the Si–CH═CH2 bending, and 963 cm^{-1} for the C═C vibrations.[49,50] The characteristic broad band of 1097–1043 cm^{-1} is further detected and attributed to the asymmetric stretching vibrations of the Si–O–Si siloxane bridge,[51] while its symmetric stretching vibrations appear at 800 cm^{-1} and its out-of-plane deformations at 412 cm^{-1}.[52] The peak at 751 cm^{-1} is attributed to Si–CH_3 bonding and Si–O–C,[53] while C–H deformation modes at 1275 cm^{-1} and 1004 cm^{-1} are most likely related to remaining Si–O–CH_3.[53,54] Thus, both the iron oxide nanoparticles and the VTES@SiO_2 have successfully modified the surface of the melamine sponges.

Before delving into the crystalline structure of the composite sponges, as mentioned in a previous work,[55] the pristine Sp sponge exhibits a broad band around 24°, indicating its amorphous structure. Some additional peaks observed in its XRD pattern were related to the sample holder. The XRD patterns of the magnetic sponges are presented in Fig. 1e. The modified composites exhibit characteristic reflections of iron oxide nanoparticles at 30.23° (202), 35.57° (311), 43.25° (400), 54.02° (422), 57.2° (511), and 62.93° (440), which are observed in all samples. In the Sp-h-m and Sp-m-h samples, the additional diffraction peak at 9.08° (110) signals the coexistence of the magnetic nanoparticles with the a-phase of VTES@SiO_2.

The 3D porous network of the sponge is successfully maintained in all the modified sponges, as evidenced by SEM analysis (Fig. 2). For the Sp-m sample (Fig. 2a), a thick layer at the branches of the sponge is observed, consisting of accumulated polyhedral nanoparticles, along with some agglomerated entities. Energy-dispersive X-ray spectroscopy detects the three elements, C, N, O, originating from the sponge and the ligands, in addition to Fe and O of the iron oxide nanoparticles.

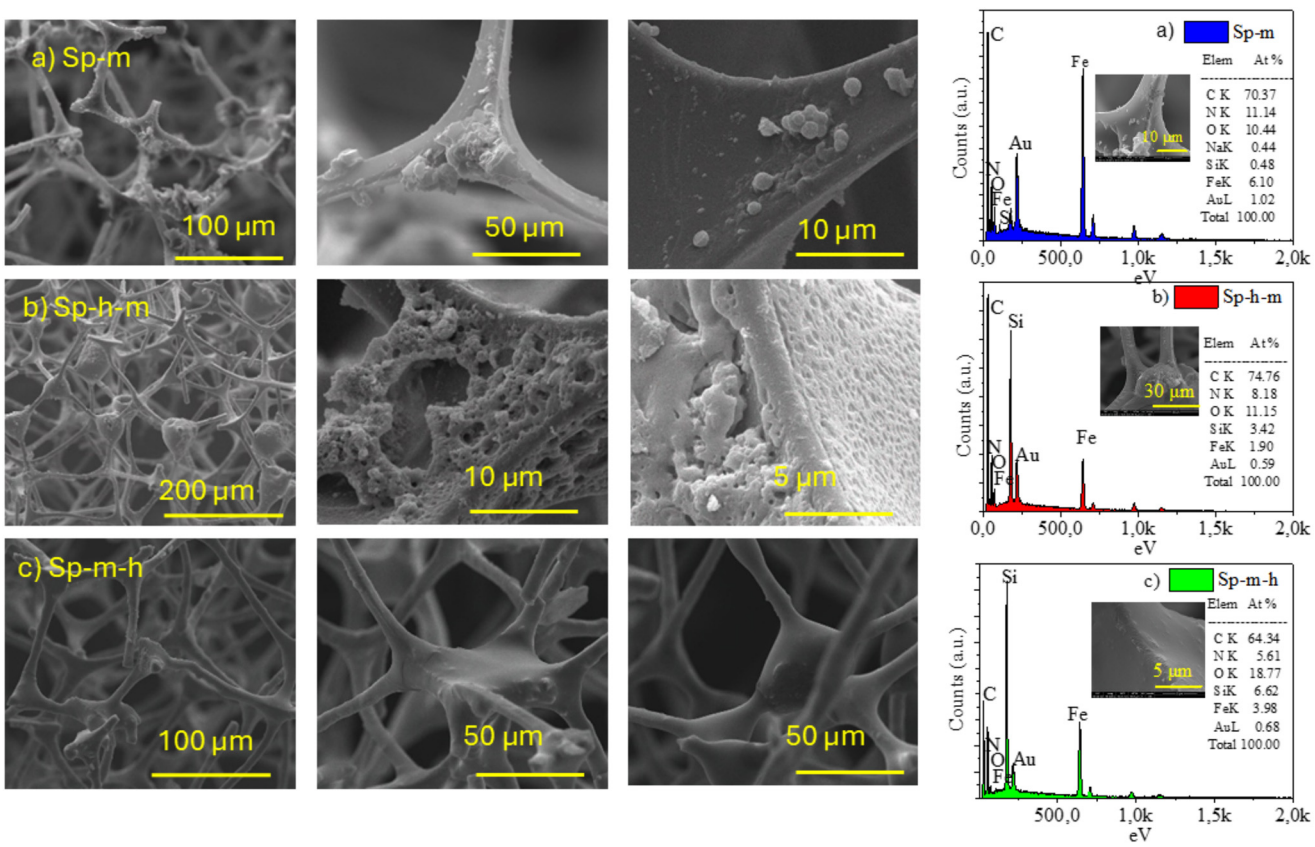

Fig. 2 SEM images and the corresponding EDX spectra of the (a) Sp-m, (b) Sp-h-m and (c) Sp-m-h samples.

In Fig. 2b, where Sp-h-m is depicted, the deposition of the iron oxide nanoparticles on the superhydrophobic sponge significantly increases the roughness of the fully covered sponge. Some compact assemblies are present at the nodes of the sponges' 3D network, and upon higher magnification, additional irregular and spherical cavities can be observed. These cavities are probably formed by the introduction of iron oxide nanoparticles and the evaporation of the dispersion solvent, offering various micro- and nanostructures on the three-dimensional sponge, which are crucial for their superhydrophobicity[56] and beneficial to adsorption applications.[57] The sample's EDX spectrum revealed all the previously identified elements, in addition to silicon, which was found in a higher percentage compared to iron.

For Sp-m-h (Fig. 2c), where VTES@SiO_2 adsorption was performed after the deposition of the iron oxide nanoparticles, a thick smooth layer grew on the surface, which could hinder the access to the iron oxide nanoparticles, protecting them. This could be useful for certain applications. Its EDX spectrum showed all the elements of the modified sponges, with a prevalence of Si over Fe. The modifications performed on the sponges were successful, allowing for the maintenance of the open pores and elasticity of the initial 3D network, which is crucial for the adsorption processes. Moreover, their surface was homogeneously covered on the interior and the exterior. The high surface roughness achieved is attributed to the hydrophobic interface of some composite sponges, resulting from their low surface energy.[34,58] These multi-hierarchical micro- and primarily nano-structures[57] may significantly benefit environmental applications for the purification of aqueous environments.

The magnetically modified sponges were submitted to magnetization measurements at room temperature to evaluate their magnetic properties. Fig. 3 shows the hysteresis magnetization loops of a sample consisting only of nanoparticles and representative samples of sponges loaded with magnetic nanoparticles. The magnetite NPs exhibit a saturation magnetization of 60 emu g^{-1} and negligible coercivity and remanence, indicating superparamagnetic behavior.[59] The saturation magnetization is higher than that reported in some other studies,[60,61] but lower than the bulk value which is to be expected for nanoparticles.[62,63]

To evaluate the magnetic behavior of sponges loaded with magnetic nanoparticles quantitatively, the reference sponges (without magnetic nanoparticles) and the sample holder were first measured to estimate the background magnetization contribution. These measurements indicate that the background magnetization varied linearly with the applied magnetic field. As a result, an appropriate linear variation of magnetization due to the background was subtracted from

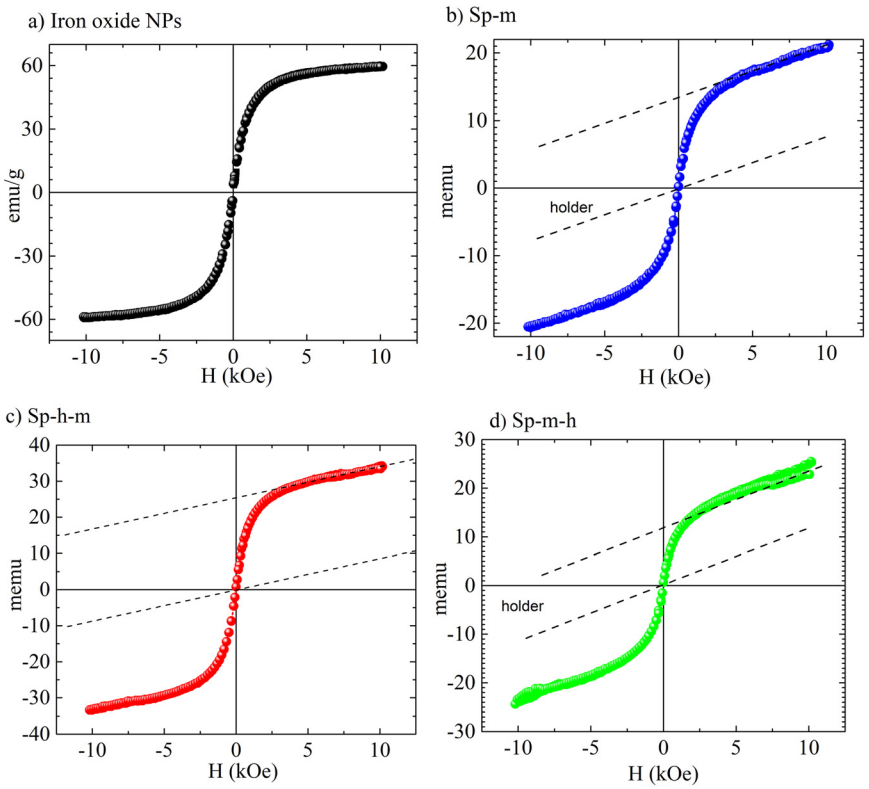

Fig. 3 Room temperature magnetic hysteresis loops for all four samples. The hysteresis curve of (a) the non-stoichiometric magnetite NPs recorded in powder form, with the *Y* axis presented in emu g^{-1}. For recording the hysteresis curves of the Sp-m, Sp-h-m and Sp-m-h samples, small pieces of the modified sponges were measured. Their magnetization is provided in memu and the contribution of the sample holders' curve is also presented for clarity (dashed lines). The modified sponges were weighed: (b) 1.5 mg Sp-m, (c) 2.2 mg Sp-h-m, and (d) 2.5 mg Sp-m-h.

the magnetic measurements of the samples containing magnetic nanoparticles. As one can see in Fig. 3b–d, the magnetization curves are typical for samples containing ferrimagnetic nanoparticles. This is experimental proof that magnetic nanoparticles are loaded into the sponges. Their saturation magnetization was found to be smaller than that of the as-synthesized nanoparticles due to mass dilution of the sponges, but nonetheless, they were still magnetically controllable (Fig. S3).

The contribution of the sample holder is subtracted as follows.

The saturation magnetic moment of the sponges shown in Fig. 3b–d at 10 kOe is estimated to be Sp-m, $\approx 11 \times 10^{-3}$ emu, Sp-h-m, $\approx 25 \times 10^{-3}$ emu, and Sp-m-h $\approx 11 \times 10^{-3}$ emu. The small saturation mass magnetization (total mass of the sponge and magnetic nanoparticles) is reasonable because of the small paramagnetic contribution of the sponge.[64,65] Although their magnetic responses vary, all magnetically modified sponges were submersed into the same volume of iron oxide nanoparticles in hexane. Different quantities may have been functionalized on the sponge in each sample, which is dependent on the preparation method of the modified sponges. Thus, the mass of the magnetic nanoparticles was determined by dividing the saturation magnetic moment of each sample by the saturation magnetization measured for the pure magnetic nanoparticles. The calculated quantity of iron oxide nanoparticles explains the differences in the magnetization of the sponges. For Sp-m and Sp-m-h, in which the deposition of the nanoparticles was the first modification step, ≈0.2 mg is attached, whereas at Sp-h-m, more sites were added owing to the VTES@SiO_2, and thus a doubled quantity of ≈0.4 mg is attached.

The Sp-h-m sample exhibits the highest saturation magnetization among the presented composites. Thus, the nanoparticles on the sponge's surface evidenced in Fig. 2b are efficiently immobilized, owing to the oleophilic nature of the superhydrophobic sponge beneath. Interestingly, the saturation magnetizations of the modified sponges presented in this work are higher than those previously reported for sponges employed in similar applications.[66]

4.2. Crude oil removal

Generally, the melamine sponges are reported to have low density (4–12 mg cm^{-3}) and high porosity (>99%),[10] which are highly beneficial for oil adsorption and removal from the water surface. In this work, the density of the pristine sponges was 7.3 mg cm^{-3}, which corresponds to 99.5% porosity, taking into account the density of bulk melamine resin of 1.51×10^{-3} mg cm^{-3}.[12,30] After the modification with the iron oxide nanoparticles and the hydrophobic silanization, the density of the sponges increased within the range of 10.5–14.2 mg cm^{-3}, whereas their porosity varies between 99% and 99.3%, as depicted in Table S1. The density of the crude oil used in this work was 0.823 g cm^{-3}.

4.2.1. Selective adsorption of oil from water. The selectivity of the magnetic sponges was evaluated by their ability to adsorb crude oil from an oil/water system with an excess of water (Fig. S4a). The modified sponges exhibited high initial adsorption capacities and fast water purification from oil spills. The adsorption capacities for the 1st cycle as per sponges' mass ($AC_{m/m}$) and volume ($AC_{m/V}$) are presented in Fig. 4. The modified sponges showed an $AC_{m/m}$ of ~83 (Sp-m), ~53 (Sp-h-m) and ~30 (Sp-m-h) mg mg^{-1}, while the pristine sponge Sp showed an $AC_{m/m}$ of ~103 mg mg^{-1}. Similarly, the $AC_{m/V}$ of the modified sponges decreased in the order Sp-m > Sp-h-m > Sp-m-h, with the $AC_{m/V}$ of Sp-m (996 mg cm^{-3}) being close to that of the pristine Sp (1031 mg cm^{-3}). Notably, the recorded adsorption capacities of the modified sponges are among the highest reported in the literature with magnetic and hydrophobic modifications.[12,26,27,30,34]

After the second cycle, the adsorbed and the desorbed quantities decreased and remained stable for the next 4 cycles. This decrease for the modified sponges could be explained by (i) the low quantity of oil remaining available on the water surface after the initial cycles, and (ii) their significant water repellency as shown by the contact angle measurements. For these samples, the total quantities Q_{ads} and Q_{des} were close to the 500 mg of oil added to the oil/water system. Importantly, after the desorption process, pure oil without any water was obtained due to their hydrophobic properties. In contrast, water was clearly observed for the pristine Sp (Fig. S4c and d), attributed to its natural hydrophilicity. During the first cycle, the Sp sample adsorbed oil too, which is not unusual given its oleophilic properties.[16] At the same time, the level of water purification (Fig. S5) was the lowest, and oil was present on the water surface even after the 6th cycle, thus confirming its low selectivity. In contrast, the modified sponges removed the entire oil quantity added to the system during the first two cycles, and after the 6th cycle, the water was clear without oil traces (Fig. S5).

4.2.2. Oil adsorption capacity and reusability. The adsorption capacity and the reusability of the sponges for oil removal were examined by the adsorption of crude oil from a system composed of a thick oil layer on the surface of water (Fig. S4b). The adsorption–desorption procedure was repeated 15 times with the sponges to release more than 99% of the adsorbed oil, as depicted in Table S1. It is important to note here that the sponges were tested without being regenerated (*i.e.* without washing with hexane to remove the oil) between the cycles. Thus, when immersed in the system, all the sponges exhibited a maximum initial oil adsorption, which was decreased after the next adsorption–desorption cycles, and became stable at around the 4th cycle. The sponges did not demonstrate significant changes after the cycles as evidenced by the optical microscopy images presented in Fig. S6.

The $AC_{m/m}$ and $AC_{m/V}$ of the sponges for the 1st cycle (initial) and for all 15 cycles (average) are compared in Fig. 4b and c. In this experiment, all the modified samples exhibited relatively high adsorption capacities per unit mass and volume of the sponge. The $AC_{m/m}$ of the Sp-m was the highest, owing to the high surface area of the magnetite NPs for oil adsorption, and

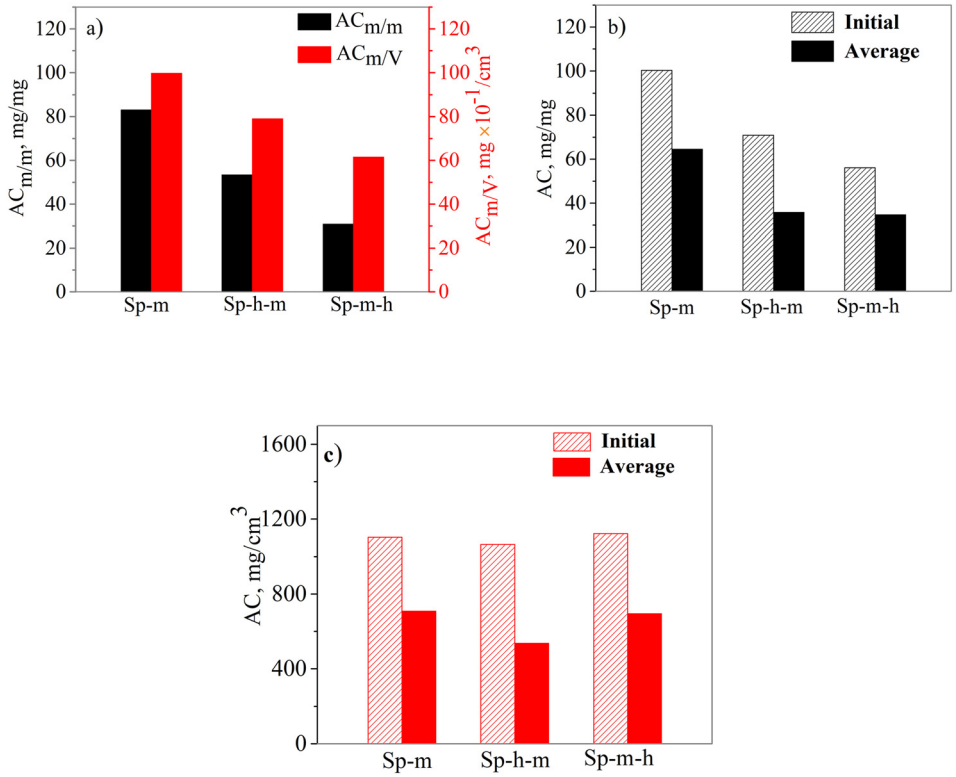

Fig. 4 For the selectivity experiment, (a) the adsorption capacities $AC_{m/m}$ and $AC_{m/V}$ of the sponges for the 1st cycle of the adsorption, (b) the gravimetric/gravimetric adsorption capacities for the 1st cycle (initial $AC_{m/m}$) and for the repeatability experiment of 15 cycles (average $AC_{m/m}$), (c) the gravimetric/volumetric adsorption capacities for the 1st cycle (initial $AC_{m/V}$) and for the 15 cycles (average $AC_{m/V}$).

reaching an initial $AC_{m/m}$ of ~100 mg mg^{-1} and average $AC_{m/m}$ of ~65 mg mg^{-1}, which are very close to the values for the pristine Sp (~117 mg mg^{-1} and ~66 mg mg^{-1}, respectively). The sponges with additional hydrophobic modification, *i.e.* Sp-h-m and Sp-m-h, exhibited lower initial $AC_{m/m}$ (~70 mg mg^{-1} and ~60 mg mg^{-1}) and average $AC_{m/m}$ of ~35 mg mg^{-1}.

All the modified sponges exhibited excellent gravimetric/volumetric AC. For the Sp-m sponge, the initial $AC_{m/V}$ was found to be ~1300 mg cm^{-3} and the average $AC_{m/V}$ was ~745 mg cm^{-3}. The Sp-h-m and the Sp-m-h sponges also showed similar or higher AC than the pristine Sp, the values of which were ~1175 mg cm^{-3} as initial and ~657 mg cm^{-3} as average $AC_{m/V}$. These findings suggest that modifying the melamine sponge with F_3O_4 through the selected route enhances the overall oil adsorption capacity of the sponge. The additional hydrophobic modification with VTES@SiO_2 nanoparticles decreases the initial oil uptake but does not significantly affect the average oil adsorbance capacity within the frame of 15 cycles. The regeneration of the sponges by washing with hexane and ethanol and drying overnight resulted in a return to ~70% of the initial AC and to ~95% of the hydrophobicity (water contact angle; WCA). It should be noted that despite the large thickness of the oil layer on the water surface, the pristine sponge Sp exhibited water release after the 5th cycle, which became more prominent after the 9th cycle. Some water release was also observed for the sponges with final magnetic modification, Sp-m and Sp-h-m, after the 7th and the 12th cycle, respectively. Such a phenomenon was not observed for the sponge with final hydrophobic modification, Sp-m-h, which makes it highly effective in oil separation from the water surface. Importantly, the sponges with both magnetic and hydrophobic properties can be maneuvered at a distance on the oil/water surface in a direction defined by an external magnetic field (Fig. S7 and S8).

In addition to establishing the magnetic response at the sponges, sufficient hydrophobicity needed to be achieved and further retained through the repeated oil adsorption/desorption cycles and their purification. The wettability of the composite's surface was evaluated through contact angle analysis, and the measured values are presented in Fig. 5. When the droplet of deionized water was shed upon the melamine sponge, it was immediately absorbed and no contact angle could be measured (not shown). This is related to its superhydrophilicity and the presence of the abundant polar groups –NH_2, N–H and –OH on the melamine's surface.[67] After the modifications of the sponges, the contact angle increases, and the surfaces exhibit superhydrophobic properties. The droplet of deionized water remained stable upon the surface. Generally, SiO_2 nanoparticles have a hydrophilic character in nature; however, when they are functionalized with a hydrophobic silane agent, they obtain superhydrophobic properties.[11] Similarly, since the magnetic nanoparticles are coated with ligands consisting of large aliphatic chains, they offer a hydrophobic interface,[68] which

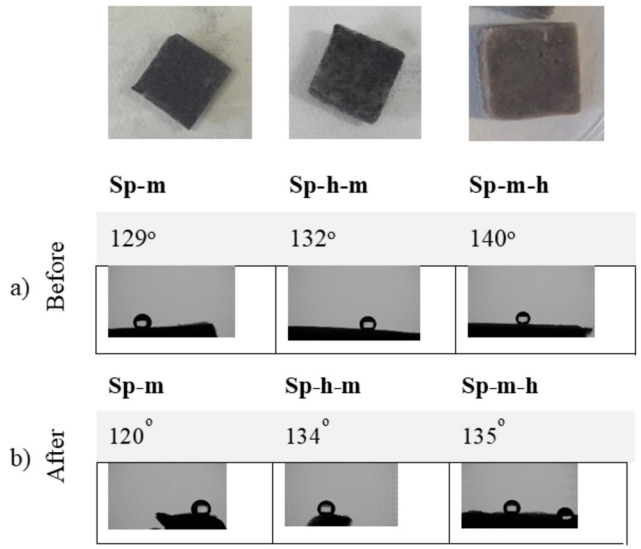

Fig. 5 (a) Photos of the Sp-m, Sp-h-m and Sp-m-h samples as well as their initial contact angles with a droplet of water and (b) the contact angles after the oil extraction and the subsequent purification process.

was expected as the dispersion is stable only in non-polar solvents. The average contact angle measured for the Sp-m sample is 129°. The contact angle of the hydrophobic and magnetic composite sponges is dependent on the sequence of their preparation (Sp-m-h and Sp-h-m). Both demonstrate higher contact angles than Sp-m, but lower than Sp-h. When the final step of the modification is the adsorption and silanization process (Sp-m-h), they have a CA of 140°, higher than of Sp-h-m with 132° CA, when the final step is the deposition of the magnetic nanoparticles. After their application in the oil removal, the sponges were rinsed with *n*-hexane in order to remove their adsorbed quantity. Their form was slightly changed after the manual desorption cycles, but their hydrophobic properties remained. In Fig. 5b, the contact angles of the sponges after the oil experiments are gathered. There was a slight decrease in the range of 5°–10°, indicating the preservation of superhydrophobicity for all modified sponges and their stability after repetitive adsorption/desorption cycles.

Overall, the recorded adsorption of ~100 g g^{-1} and repeatability of ~65 g g^{-1} for 15 cycles are among the highest published in the literature for different types of sponges.[26,27,30,69,70] In our work, the performance is attributed to the synergy of the selected modifiers of the sponge's surface. Specifically, the silicon oxide mediator (SiO_2) is readily attached on the sponge and is subsequently modified with the hydrophobic silane (VTES), thus guaranteeing high stability and hydrophobicity. In addition, the use of magnetic nanoparticles modified with large aliphatic chains allows their immobilization on the sponge's skeleton, providing magnetic response and hydrophobicity. Moreover, the deposition of VTES@SiO_2 as a final coating onto Sp-m (see Fig. 2c) further stabilizes the nanoparticles and increases the water repellence, thus leading to the superior performance of Sp-m-h, which demonstrated the highest number of adsorption cycles without uptake of water.

4.3. Heavy metal removal: mercury and arsenic

Evaluation of heavy metal ion removal from water. Furthermore, both pristine and modified sponges were evaluated regarding their ability to remove the heavy metal ions Hg^{2+} and As^{3+} from single metal ion aqueous solutions under dynamic conditions of 60 min total time.

The sorbed metal content (q, mg g^{-1}) by the modified sponges (eqn (3)) and the removal percentage (%) (eqn (4)) of the examined metals from the aqueous solutions were defined as follows:

$$q = (C_0 - C)\frac{V}{m} \quad (3)$$

$$\text{Removal}\ (\%) = \frac{(C_0 - C)}{C_0} \times 100 \quad (4)$$

where C_0 and C are the initial and final solute metal concentration (mg L^{-1}), V is the volume of the solution (L), and m is the mass of the modified sponges (g). Each data point was calculated as the mean value between the three replicate columns at the same time interval, while the error bars represent the relative difference of the measurements.

The sponges (Sp-h-m, Sp-m and Sp-m-h) were applied to adsorb metal ions. Fig. 6a indicates the experimental data for the adsorption of As^{3+} and Hg^{2+} using single metal ion aqueous solutions (the concentration of each metal ion was

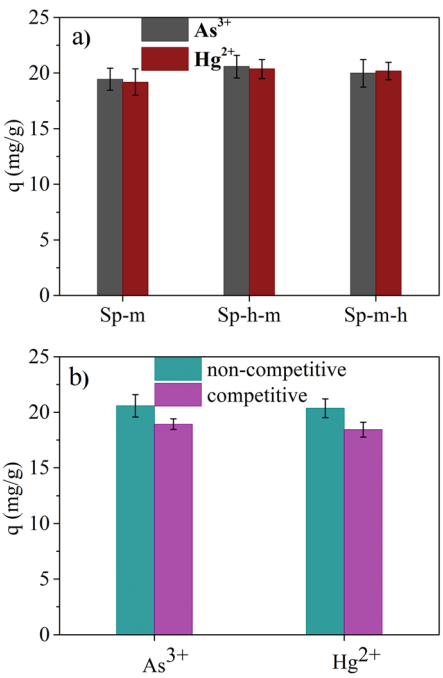

Fig. 6 (a) The adsorbed quantities of As^{3+} and Hg^{2+} in mg g^{-1} of Sp-m, Sp-h-m and Sp-m-h sponges in the experiments of single metal ion solutions and (b) the adsorbed As^{3+} and Hg^{2+} on the Sp-h-m sponge in the experiment of competitive adsorption.

fixed at 250 ppm) on the examined sponges. Based on the acquired results, the Sp-h-m sponge exhibited the highest adsorption capacity for both heavy metals. More specifically, its adsorption capacity towards As^{3+} and Hg^{2+} was 20.5 and 20.3 mg g^{-1}, respectively, which decreased to 19.9 (As^{3+}) and 20.1 (Hg^{2+}) mg g^{-1} for Sp-m-h and further to 19.4 (As^{3+}) and 19.2 (Hg^{2+}) mg g^{-1} in the case of the Sp-m sponge. It is possible that Sp-h-m demonstrates the highest adsorption capacity, as a synergetic effect exists between the magnetic and the hydrophobic modifications of the sponge. As seen from SEM, lots of cavities are present that can permit the diffusion of metal ions to both iron oxide nanoparticles and VTES@SiO_2, which further enhances the accessible surface area for the adsorption. Moreover, its higher saturation magnetization among the modified sponges can influence the attraction and simultaneous extraction of metal ions from the aqueous solution. The Sp-m sponge previously presented the best oil removal due to the large surface of iron oxide nanoparticles, but in the metal removal application, it seems to have the lowest capacity. On the Sp-m-h sponge, VTES@SiO_2 covered the NPs and blocked the available surface. Phase changes due to further oxidation of magnetite could have also altered the properties, in addition to the higher oxygen content. The interactions driven by the cooperation of these functional groups enrich the mechanism of adsorption, from physical adsorption and electrostatic interactions to hydrogen bonding and surface complexation.[67,68]

In addition to the singe metal ion experiment (non-competitive system) the Sp-h-m sponge, which indicated the most enhanced capacity, was submitted to an additional experiment. A mixed metal ion aqueous solution was prepared with 250 ppm concentration of each As^{3+} and Hg^{2+} ion (total 500 ppm of toxic metals). The results are compared and presented in Fig. 6b. The adsorption capacity of the Sp-h-m sponge towards As^{3+} and Hg^{2+} in the competitive conditions decreased in the mixed solution, in relation to the adsorption values for the single metal ion solutions. With these competitive conditions, the adsorption values were 18.9 and 18.4 mg g^{-1} against As^{3+} and Hg^{2+}, respectively. Compared with the adsorption values of the single metal ion solutions, the adsorption capacity is slightly affected due to the competition of one metal ion with the other to occupy the modified sponge's sites, decreasing by about 8% for As^{3+} and by 9.4% for Hg^{2+}. It is thus concluded that close to 500 ppm As^{3+} and Hg^{2+} together were adsorbed overall effectively. Iron oxide nanoparticles are excellent platforms for sorption of heavy metal cations, while both the pristine sponge and the silica layer can facilitate water purification processes. The efficiency of the magnetite crystals that are employed in our work is proven by the fact that the Sp-m sample that does not contain silica layers already adsorbs both Hg(II) and As(III). In previous studies, Faulconer *et al.* utilized iron oxide nanomaterials which achieved excellent Hg(II) removal efficiency. The proposed adsorption process involved a strong binding affinity of the iron oxide surface with divalent mercury ions through coordination with oxygen atoms.[71] Arsenic removal poses a more complicated picture in the literature due to the stability of both As^{3+} and As^{5+} cations, two forms that may coexist due to redox reactions with the nanoparticles, as in the case of zero-valent iron NPs. In a comprehensive paper by Wei *et al.*, it was revealed that the ionic strength of the solution had a negligible effect on the adsorption of both As^{3+} and As^{5+} in iron oxide nanoneedles.[72] Furthermore, our work indicates that there is no competition between the two heavy metals in terms of adsorption capacity (see Fig. 6b). The latter, coupled with the fact the adsorption capacity is rather similar, indicates an adsorption mechanism through interaction with under-coordinated oxygen sites. The pH of the solution is acidic; hence we exclude the formation of hydroxide species with reduced solubility and removal of the heavy metals is due to adsorption by the modified sponges. By this straightforward preparation method of these multifunctional magnetic hydrophobic sponges compared to others,[73,74] both ions present in the solution are adsorbed in high quantities in only 60 min. Typical regeneration processes involve mild treatment with 2 M NaOH solution[75] for arsenic adsorption and electrolysis for mercury.[76] To that end, even small pieces of the magnetically controllable sponge can efficiently lead to the purification of water systems to the levels required by the World Health Organization (0.01 ppm for As and 0.006 ppm for Hg) and the United States Environmental Protection Agency (0.01 ppm for As and 0.002 ppm for Hg). Notably, according to our cost and scalability evaluation (not presented here), the large-scale synthesis and commercialization of the developed magnetic hydrophobic sponges is totally feasible due to the low-cost raw materials and processing.

Conclusions

A large-scale synthesis of iron oxide nanoparticles with hydrophobic chains was accomplished in a one-step thermolytic reaction prior to their incorporation on pristine and hydrophobic modified sponges. The phase composition of the nanoparticles with a size lower than 18 nm consisted of non-stoichiometric magnetite with a saturation magnetization of 60 emu g^{-1}. The modification of the chemical composition and morphology of the sponges was achieved by their straightforward immersion in ferrofluid solution. The new micro- and nanostructures obtained by three different methods exhibited exquisite magnetic properties, which benefited the removal of both crude oil and heavy metals from aqueous environments. The modified magnetic sponges exhibited high adsorption capacity (60–100 g g^{-1}) and high selectivity to oil that was attributed to their strong hydrophobic behavior (WCA 140°), allowing only oil adsorption. This behavior was more pronounced when VTES@SiO_2 nanoparticles were deposited as the last layer, thus exposing the hydrophobic vinyl terminations to the oil–water interface, achieving greater water repellency. The

efficiency of Sp-m was also noticeable due to its high surface area for oil adsorption. The surface hydrophobicity of all magnetically modified sponges was retained after repetitive cycles of application. New synergetic effects have arisen from both VTES@SiO_2 and Fe_3O_4, creating additional cavities, offering higher magnetization and more functional groups available for the metal ions, which contributed to the high efficiency of Sp-h-m, adsorbing 250 ppm in a single ion solution of As^{3+} and Hg^{2+} in 60 min. This modified sponge also demonstrated excellent performance when both 250 ppm As^{3+} and 250 ppm Hg^{2+} were present in the solution during the competitive metal ion system. Thus, the sequence of the modification steps influences the performance of the magnetic modified sponges dependent on the application. This finding allows preparation and optimization of effective adsorbing materials for specific water purification applications, *i.e.* crude oil or heavy metal ion (As^{3+} and Hg^{2+}) adsorption.

Author contributions

P. B.: conceptualization, methodology, formal analysis, investigation, data curation, writing – original draft. N. T.: conceptualization, methodology, formal analysis, investigation, data curation, writing – original draft. M. P.: formal analysis, investigation, writing – original draft. E. D.: formal analysis, investigation, writing – original draft. E. S.: investigation. N. B.: investigation. E. A. P.: methodology, investigation, writing – original draft, writing-review and editing. M.-A. G.: methodology, investigation, writing – original draft, writing – review and editing. N. L.: writing – original draft, writing – review and editing. T. L.: investigation, writing – review and editing. L.-A. T.: investigation, writing – review and editing. V. K. T.: conceptualization, methodology, investigation, visualization, writing – original draft. P. D.: conceptualization, methodology, formal analysis, investigation, writing-original draft, supervision, visualization, project administration.

Conflicts of interest

There are no conflicts to declare.

Data availability

Data for this article are either included in the manuscript or available upon request to the corresponding authors.

Supplementary information (SI): captures of the ferrofluid and the magnetic modified sponges with the application of an external magnetic field out and in an oil/water system; table of the data derived from the selectivity and oil capacitance experiments along with their photos and videos, size distribution diagram for the iron oxide nanoparticles and optical microscopy images for the Sp-h-m sample. See DOI: https://doi.org/10.1039/d5en00549c.

Acknowledgements

We acknowledge the support from the project 'ATTP4 0359579 COF4SEA' (MIS 5217185) co-financed by the European Union and Greek National Funds through the Operational Program ATTIKA 2014-2020, under the call Research and Innovation Cooperations in the Region of Attica. We acknowledge Dr. Dimitrios Tsoukleris and NanoViis Innovative Nanotechnologies as coordinators of the project 'ATTP4 0359579 COF4SEA' (MIS 5217185). We are also grateful to Dr. V. Psycharis and the Crystallography and Coordination Chemistry Materials laboratory.

References

1 United States Environmental Protection Agency, *Understanding Oil Spills And Oil Spill Response*, 540-K-99-007 OSWER 9200.5-104A PB2000-963401, December 1999.
2 K. Sharma, G. Shah, K. Singhal and V. Soni, Comprehensive insights into the impact of oil pollution on the environment, *Reg. Stud. Mar. Sci.*, 2024, **74**, 103516.
3 E. M. Hadji, B. Fu, A. Abebe, H. M. Bilal and J. Wang, Sponge-based materials for oil spill cleanups: A review, *Front. Chem. Sci. Eng.*, 2020, **14**, 749–762.
4 L. Peng, S. Yuan, G. Yan, P. Yu and Y. Luo, Hydrophobic Sponge for Spilled Oil Absorption, *J. Appl. Polym. Sci.*, 2024, 40889.
5 Z.-T. Li, H.-T. Wu, W.-Y. Chen, F.-A. He and D.-H. Li, Preparation of magnetic superhydrophobic melamine sponges for effective oil-water separation, *Sep. Purif. Technol.*, 2019, **212**, 40–50.
6 H. Zhu, D. Chen, S. Yang, N. Li, Q. Xu, H. Li, L. Wang, J. He, J. Jiang and J. Lu, A versatile and cost-effective reduced graphene oxide-crosslinked polyurethane sponge for highly effective wastewater treatment, *RSC Adv.*, 2016, **6**, 38350.
7 S. M. Kong, Y. Han, N.-I. Won and Y. H. Na, Polyurethane Sponge with a Modified Specific Surface for Repeatable Oil –Water Separation, *ACS Omega*, 2021, **6**, 33969–33975.
8 I. Riyal, G. Joshi, H. Sharma and C. Dwivedi, Modified hydrophobic and oleophilic polyurethane sponge for oil absorption with MIL-53, *Environ. Res.*, 2023, **237**, 116982.
9 Z. Han, X. Lv, Y. Li, M. Gao, Z. Tang, X. Su, Z. Zhang, H. Li, J. He, Z. Zheng and Y. Liu, Preparation of Superhydrophobic and Multifunctional Sponges for Oil/Water Separation and Oil Absorption, *Langmuir*, 2024, **40**, 23902–23917.
10 V. H. Pham and J. H. Dickerson, Superhydrophobic Silanized Melamine Sponges as High Efficiency Oil Absorbent Materials, *ACS Appl. Mater. Interfaces*, 2014, **6**, 14181–14188.
11 H. Gao, P. Sun, Y. Zhang, X. Zeng, D. Wang, Y. Zhang, W. Wang and J. Wu, Two-step hydrophobic fabrication of melamine sponge for oil absorption and oil/water separation, *Surf. Coat. Technol.*, 2018, **339**, 147–154.
12 Y. Ding, W. Xu, Y. Yu, H. Hou and Z. Zhu, One-Step Preparation of Highly Hydrophobic and Oleophilic Melamine Sponges via Metal-Ion-Induced Wettability Transition, *ACS Appl. Mater. Interfaces*, 2018, **10**, 6652–6660.

13 E. Piperopoulos, L. Calabrese, E. Mastronardo, C. Milone and E. Proverbio, Carbon-based sponges for oil spill recovery, *Carbon Nanomaterials for Agri-Food and Environmental Applications, Micro and Nano Technologies*, 2020, pp. 155–175.

14 J. Cao, Y. Wang, D. Wang, R. Sun, M. Guo and S. Feng, A Super-Amphiphilic 3D Silicone Sponge with High Porosity for the Efficient Adsorption of Various Pollutants, *Macromol. Rapid Commun.*, 2021, **42**, 2000603.

15 C. Zhang, T. Cai, S. Ge-Zhang, P. Mu, Y. Liu and J. Cui, Wood Sponge for Oil–Water Separation, *Polymer*, 2024, **16**, 2362.

16 X. Zhou, D. Li, L. Wang, Q. Wang, Z. Wang, Q. Jing, R. Marisol and L. Li, Recent advances in the modification of melamine sponge for oil-water separation, *J. Mater. Sci. Technol.*, 2025, **207**, 209–224.

17 R. Zhang, Z. Zhou, W. Ge, Y. Lu, T. Liu, W. Yang and J. Dai, Robust, fluorine-free and superhydrophobic composite melamine sponge modified with dual silanized SiO_2 microspheres for oil–water separation, *Chin. J. Chem. Eng.*, 2021, **33**, 50–60.

18 Y. Fang, L. Yan and H. Liu, Facile Preparation of Hydrophobic Melamine Sponges using Naturally Derived Urushiol for Efficient Oil/Water Separation, *ACS Appl. Polym. Mater.*, 2020, **2**, 3781–3788.

19 Q.-R. Xiao, P. Xu, S. Sun, X.-L. Qiang and X.-L. Shi, Facile fabrication of ink-based conductive hydrophobic melamine sponge for oil/water separation and oils detection, *Appl. Surf. Sci.*, 2022, **604**, 154532.

20 E.-C. Cho, C.-W. Chang-Jian, Y.-S. Hsiao, K.-C. Lee and J.-H. Huang, Interfacial engineering of melamine sponges using hydrophobic TiO_2 nanoparticles for effective oil/water separation, *J. Taiwan Inst. Chem. Eng.*, 2016, **67**, 476–483.

21 H. Wu, L. Hao, C. Chen and J. Zhou, Superhydrophobic Fe_3O_4/OA Magnetorheological Fluid for Removing Oil Slick from Water Surfaces Effectively and Quickly, *ACS Omega*, 2020, **5**, 27425–27432.

22 L. Qiao, Z. Zhou, M. Wang and Z. He, Lignin Microsphere/TiO_2 Composite-Based Melamine Sponge with Superhydrophobic and Photothermal Properties for Oil/Water Separation and Anti-Icing, *Langmuir*, 2024, **40**(11), 5978–5991.

23 Y. Chen, Y. Zhao, W. Yang and Z. Su, Solar-heated melamine sponge decorated with Fe3O4 for continuous recovery of viscous crude oil, *J. Porous Mater.*, 2024, **31**(3), 937–943.

24 M. Wang, L. Qiao, S. Ma and Z. He, Facile Preparation of Photothermal Superhydrophobic Melamine Sponge Decorated with MXene and Lignin Particles for Efficient Oil/Water Separation, Fast Crude Oil Recovery, and Active Deicing, *Langmuir*, 2025, **41**(21), 13233–13248.

25 J. Zhao, Q. Guo, X. Wang, H. Xie and Y. Chen, Recycle and reusable melamine sponge coated by graphene for highly efficient oil-absorption, *Colloids Surf., A*, 2016, **488**, 93–99.

26 H. Si, Q. Liu, Z. Fan, B. Wang, Q. Tong and M. Lin, A Durable Magnetic Superhydrophobic Melamine Sponge: For Solving Complex Marine Oil Spills, *Nanomaterials*, 2022, **12**, 2488.

27 Y. Zhang, P. Wang, T. Zhang, X. Hu, H. Shao and X. Guo, Improved superhydrophobicity of melamine sponge by aminosilane for batch and continuous oil-water separation, *Chem. Eng. Sci.*, 2025, **303**, 120996.

28 Y. Guan, Z. Wang, M. Bao, X. Chen, L. Dong, Y. Shen and Y. Li, Multi-energies assisted and all-weather recovery of crude oil by superhydrophobic melamine sponge, *J. Hazard. Mater.*, 2023, **443**, 130131.

29 H. Dong, Y. Zhan, A. Sun, Y. Chen and X. Chen, Magnetically responsive and durable super-hydrophobic melamine sponge material, *Colloids Surf., A*, 2023, **662**, 130933.

30 P. Makos-Chełstowska, E. Słupek, A. Mielewczyk-Gryn and T. Klimczuk, Magnetic superhydrophobic melamine sponges for crude oil removal from water, *Chemosphere*, 2024, **346**, 140533.

31 Z. Yina, Y. Li, T. Song, M. Bao, Y. Li, J. Lu and Y. Li, An environmentally benign approach to prepare superhydrophobic magnetic melamine sponge for effective oil/water separation, *Sep. Purif. Technol.*, 2020, **236**, 116308.

32 C.-H. Chung, W.-C. Liu and J.-L. Hong, Superhydrophobic Melamine Sponge Modified by Cross-Linked Urea Network as Recyclable Oil Absorbent Materials, *Ind. Eng. Chem. Res.*, 2018, **57**, 8449–8459.

33 X. Dong, M. Cui, R. Huang, R. Su, W. Qi and Z. He, Polydopamine-Assisted Surface Coating of MIL-53 and Dodecanethiol on a Melamine Sponge for Oil–Water Separation, *Langmuir*, 2020, **36**, 1212–1220.

34 Z.-T. Li, H.-T. Wu, W.-Y. Chen, F.-A. He and D.-H. Li, Preparation of magnetic superhydrophobic melamine sponges for effective oil-water separation, *Sep. Purif. Technol.*, 2019, **212**, 40–50.

35 R. Zhang, Z. Zhou, W. Ge, Y. Lu, T. Liu, W. Yang and J. Dai, Robust, fluorine-free and superhydrophobic composite melamine sponge modified with dual silanized SiO_2 microspheres for oil–water separation, *Chin. J. Chem. Eng.*, 2021, **33**, 50–60.

36 N. A. A. Qasem, R. H. Mohammed and D. U. Lawal, Removal of heavy metal ions from wastewater: a comprehensive and critical review, *npj Clean Water*, 2021, **4**, 36.

37 S. V. Saghir and E. K. Goharshadi, Multifunctional MnO_2 nanorods-modified wood sponge for water remediation: applications for heavy metal sorption and oil/water separation, *Wood Sci. Technol.*, 2024, **58**, 2097–2113.

38 L. Wang, J. Li, Q. Jiang and L. Zhao, Water-soluble Fe_3O_4 nanoparticles with high solubility for removal of heavy-metal ions from waste water, *Dalton Trans.*, 2012, **41**, 4544–4551.

39 V. K. Tzitzios, A. Bakandritsos, V. Georgakilas, G. Basina, N. Boukos, A. B. Bourlinos, D. Niarchos and D. Petridis, Large-scale synthesis, size control, and anisotropic growth of gamma-Fe_2O_3 nanoparticles: organosols and hydrosols, *J. Nanosci. Nanotechnol.*, 2007, **7**(8), 2753–2757.

40 A. P. Douvaris, A. Polymeros and T. Bakas, IMSG-09: A ^{57}Fe–^{119}Sn Mössbauer spectra computer fitting program with novel interactive user interface, *J. Phys.:Conf. Ser.*, 2010, **217**, 012014.

41 S. Mourdikoudis, M. Menelaou, N. Fiuza-Maneiro, G. Zheng, S. Wei, J. Pérez-Juste, L. Polavarapu and Z. Sofer, Oleic acid/

oleylamine ligand pair: a versatile combination in the synthesis of colloidal nanoparticles, *Nanoscale Horiz.*, 2022, **7**, 941.

42 C. F. Holder and R. E. Schaak, Tutorial on powder X-ray diffraction for characterizing nanoscale materials, *ACS Nano*, 2019, **13**, 7359–7365.

43 S. Sun and H. Zeng, Size-Controlled Synthesis of Magnetite Nanoparticles, *J. Am. Chem. Soc.*, 2002, **124**(28), 8204–8205.

44 H. Sharifi Dehsari, V. Ksenofontov, A. Möller, G. Jakob and K. Asadi, Determining Magnetite/Maghemite Composition and Core-Shell Nanostructure from Magnetization Curve for Iron Oxide Nanoparticles, *J. Phys. Chem. C*, 2018, **122**(49), 28292–28301.

45 A. L. Flores, N. Medina-Berríos, W. Pantoja-Romero, D. B. Plaza, K. Kisslinger, J. Beltran-Huarac, G. Morell and B. R. Weiner, Geometry and Surface Area Optimization in Iron OxideNanoparticles for Enhanced Magnetic Properties, *ACS Omega*, 2024, **9**, 32980–32990.

46 G. Basina, G. Mountrichas, E. Devlin, N. Boukos, D. Niarchos, D. Petridis, S. Pispas and V. Tzitzios, Synthesis and Magnetic Properties of Fe_3O_4 Nanoparticles Coated with Biocompatible Double Hydrophilic Block Copolymer, *J. Nanosci. Nanotechnol.*, 2009, **9**(8), 4753–4759.

47 J. Ibarra, J. Melendres, M. Almada, M. G. Burboa, P. Taboada, J. Juárez and M. A. Valdez, Synthesis and characterization of magnetite/PLGA/chitosan nanoparticles, *Mater. Res. Express*, 2015, **2**, 095010.

48 A. B. Bourlinos, A. Bakandritsos, V. Georgakilas, V. Tzitzios and D. Petridis, Facile synthesis of capped c-Fe2O3 and Fe3O4 nanoparticles, *J. Mater. Sci.*, 2006, **41**, 5250–5256.

49 N. Khurana, P. Arora, A. S. Pente, K. C. Pancholi, V. Kumar, C. P. Kaushik and S. Rattan, Surface modification of zinc oxide nanoparticles by vinyltriethoxy silane (VTES), *Inorg. Chem. Commun.*, 2021, **124**, 108347.

50 L. M. Johnson, L. Gao, C. W. Shields IV, M. Smith, K. Efimenko, K. Cushing, J. Genzer and G. P. López, Elastomeric microparticles for acoustic mediated bioseparations, *J. Nanobiotechnol.*, 2013, **11**, 22.

51 B. Shi, L. Xie, B. Ma, Z. Zhou, B. Xu and L. Qu, Preparation and Properties of Highly Transparent SiO_2 Aerogels for Thermal Insulation, *Gels*, 2022, **8**(11), 744.

52 R. Ellerbrock, M. Stein and J. Schaller, Comparing amorphous silica, short-range-ordered silicates and silicic acid species by FTIR, *Sci. Rep.*, 2022, **12**, 11708.

53 C. A. Canaria, I. N. Lees, A. W. Wun, G. M. Miskelly and M. J. Sailor, Characterization of the carbon–silicon stretch in methylated porous silicon—observation of an anomalous isotope shifts in the FTIR spectrum, *Inorg. Chem. Commun.*, 2002, **5**, 560–564.

54 S. Yi, Y. Su and Y. Wan, Preparation and characterization of vinyltriethoxysilane (VTES) modified silicalite-1/PDMS hybrid pervaporation membrane and its application in ethanol separation from dilute aqueous solution, *J. Membr. Sci.*, 2010, **360**, 341–351.

55 P. Bika, N. Ioannidis, P. Tsipas, S. Papagiannis, M.-A. Gatou, E. A. Pavlatou, A. G. Karydas, T. Stergiopoulos and P. Dallas, Detection and Selective Sorption of Copper Ions by a COF-Modified Melamine Sponge, *ACS Omega*, 2025, **10**, 21755–21766.

56 T. Chen, S. Zhou, Z. Hu, X. Fu, Z. Liu, B. Su, H. Wan, X. Du and Z. Gao, A multifunctional superhydrophobic melamine sponge decorated with Fe_3O_4/Ag nanocomposites for high efficient oil-water separation and antibacterial application, *Colloids Surf., A*, 2021, **626**, 127041.

57 H. Wang, Q. Zhao, K. Zhang, F. Wang, J. Zhi and C.-X. Shan, Superhydrophobic Nanodiamond-Functionalized Melamine Sponge for Oil/Water Separation, *Langmuir*, 2022, **38**, 11304–11313.

58 T. Yu, F. Halouane, D. Mathias, A. Barras, Z. Wang, A. Lv, S. Lu, W. Xu, D. Meziane, N. Tiercelin, S. Szunerits and R. Boukherrou, Preparation of magnetic, superhydrophobic/superoleophilic polyurethane sponge: Separation of oil/water mixture and demulsification, *Chem. Eng. J.*, 2020, **384**, 123339.

59 R. d. J. A. Fidelis, M. Pires, D. S. de Resende, G. F. C. Lima, P. R. P. de Paiva and A. C. d. S. Bezerra, Magnetite: Properties and applications – A review, *J. Magn. Magn. Mater.*, 2025, **614**, 172770.

60 Y. Hadadian, H. Masoomi, A. Dinari, C. Ryu, S. Hwang and S. Kim, From Low to High Saturation Magnetization in Magnetite Nanoparticles: The Crucial Role of the Molar Ratios Between the Chemicals, *ACS Omega*, 2022, **7**(18), 15996–16012.

61 R. Patil, P. Shete, N. D. Thorat, S. V. Otari, K. C. Barick, A. Prasad, R. S. Ningthoujam, B. M. Tiwale and S. H. Pawar, Superparamagnetic iron oxide/chitosan core/shells for hyperthermia application: Improved colloidal stability and biocompatibility, *J. Magn. Magn. Mater.*, 2014, **355**, 22–30.

62 A. Demortière, P. Panissod, B. P. Pichon, G. Pourroy, D. Guillon, B. Donnio and S. Bégin-Colin, Size-dependent properties of magnetic iron oxide nanocrystals, *Nanoscale*, 2011, **3**, 225–232.

63 S. J. Kemp, R. M. Ferguson, A. P. Khandhara and K. M. Krishnan, Monodisperse magnetite nanoparticles with nearly ideal saturation magnetization with higher sizes, *RSC Adv.*, 2016, **6**, 77452–77464.

64 L. Wu, L. Li, B. Li, J. Zhang and A. Wang, Magnetic, Durable, and Superhydrophobic Polyurethane@Fe_3O_4@SiO_2@Fluoropolymer Sponges for Selective Oil Absorption and Oil/Water Separation, *ACS Appl. Mater. Interfaces*, 2015, **7**, 4936–4946.

65 J. Fang, H. Wang, Y. Xue, X. Wang and T. Lin, Magnet-Induced Temporary Superhydrophobic Coatings from One-Pot Synthesized Hydrophobic Magnetic Nanoparticles, *ACS Appl. Mater. Interfaces*, 2010, **2**(5), 1449–1455.

66 Z.-T. Li, B. Lin, L.-W. Jiang, E.-C. Lin, J. Chen, S.-J. Zhang, Y.-W. Tang and F.-A. He, De-Hao L, Effective preparation of magnetic superhydrophobic Fe_3O_4/PU sponge for oil-water separation, *Appl. Surf. Sci.*, 2018, **427**, 56–64.

67 Q. Song, J. Zhu, X. Niu, J. Wang, G. Dong, M. Shan, B. Zhang, H. Matsuyama and Y. Zhang, Interfacial assembly of micro/nanoscale nanotube/silica achieves superhydrophobic

melamine sponge for water/oil separation, *Sep. Purif. Technol.*, 2022, **280**, 119920.

68 H. Li, H. Jin and R. Li, *et al.*, Magnetic Fe_3O_4@SiO_2 study on adsorption of methyl orange on nanoparticles, *Sci. Rep.*, 2024, **14**, 1217.

69 J. Chen, M. Sun, Y. Ni, T. Zhu, J. Huang, X. Li and Y. Lai, Superhydrophobic polyurethane sponge for efficient water-oil emulsion separation and rapid solar-assisted highly viscous crude oil adsorption and recovery, *J. Hazard. Mater.*, 2023, **445**, 130541.

70 L. Qiao, M. Wang, Z. Zhou and Z. He, Non-fluorinated and photothermal lignin microspheres/candle soots-based superhydrophobic sponge for crude oil recovery and separation of oil/water mixtures and emulsions, *J. Hazard. Mater.*, 2025, **495**, 138909.

71 E. K. Faulconer, N. V. Hoogesteijn von Reitzenstein and D. W. Mazyck, Optimization of magnetic powdered activated carbon for aqueous Hg(II) removal and magnetic recover, *J. Hazard. Mater.*, 2012, **199–200**, 9–14.

72 Y. Wei, S. Wei, C. Liu, T. Chen, Y. Tang, J. Ma, K. Yin and S. Luo, Efficient removal of arsenic from groundwater using iron oxide nanoneedle array-decorated biochar fibers with high Fe utilization and fast adsorption kinetics, *Water Res.*, 2019, **167**, 115107.

73 Y. Song, Z. Liu and Q. Zhang, Engineering the future: Unveiling novel paths in heavy metal wastewater remediation with advanced carbon-based nanomaterials – Beyond performance comparison, tackling challenges, and exploring opportunities, *Chemosphere*, 2024, **366**, 143477.

74 B. E. Keshta, A. H. Gemeay, D. K. Sinha, S. Elsharkawy, F. Hassan, N. Rai and C. Arora, State of the art on the magnetic iron oxide Nanoparticles: Synthesis, Functionalization, and applications in wastewater treatment, *Results Chem.*, 2024, **7**, 101388.

75 Y. Wang, L. Zhang, C. Guo, Y. Gao, S. Pan, Y. Liu, X. Li and Y. Wang, Arsenic removal performance and mechanism from water on iron hydroxide nanopetalines, *Sci. Rep.*, 2022, **12**, 17264.

76 Z. Hu, U. Kurien, K. Murwira, A. Ghoshdastidar, O. Nepotchatykh and P. A. Ariya, Development of a Green Technology for Mercury Recycling from Spent Compact Fluorescent Lamps Using Iron Oxides Nanoparticles and Electrochemistry, *ACS Sustainable Chem. Eng.*, 2016, **4**(4), 2150.